Available online at www.sciencedirect.com
ScienceDirect
Journal of Photochemistry and Photobiology A: Chemistry 195 (2008) 156–166
Journal of Photochemistry and Photobiology A:Chemistry
www.elsevier.com/locate/jphotochem

Time resolved resonance Raman, transient diffuse reflectance and kinetic studies of species generated by UV laser photolysis of biphenyl occluded within dehydrated Y-faujasite zeolites

I. Batonneau-Gener [a], Alain Moissette [b,*], Claude Brémard [b], Guy Buntinx [b]

[a] *Laboratoire de Catalyse en Chimie Organique, UMR-CNRS 6503, Université de Poitiers, 40 avenue du recteur Pineau, 80022 Poitiers, France*
[b] *Laboratoire de Spectrochimie Infrarouge et Raman UMR-CNRS 8516, Centre d' Etudes et de Recherches Lasers et Applications (FR-CNRS 2416), Bât. C5 Université des Sciences et Technologies de Lille, 59655 Villeneuve d'Ascq cedex, France*

Received 19 June 2007; received in revised form 18 September 2007; accepted 29 September 2007
Available online 5 October 2007

Abstract

Transient diffuse reflectance UV–vis absorption (TDRUV) and time resolved resonance Raman (TR^3) spectroscopy (370 nm exciting laser line, 8 ns) were performed to investigate the species generated by UV pulsed laser photolysis (248 nm, 20 ns) of biphenyl (BP) occluded in cavities of dehydrated silica-rich Y-faujasitic (M_nFAU) zeolites with $M_n(AlO_2)_n(SiO_2)_{192-n}$ formulae per unit cell. The TDRUV spectra were recorded in the time range 0.5–340 μs and the TR^3 spectra were recorded in the 0.05–100 μs as functions of aluminum content ($n = 0, 56$), extra framework cations ($M = Na^+, K^+, Cs^+$), BP loading (1, 2, 4, 8, 16 BP/UC) and laser energy (0.15–1.5 mJ). Specific spectra of $BP(T_1)$ triplet state, $BP^{\bullet+}$ radical cation, trapped electron as Na_4^{3+} cluster and $BP^{\bullet-}$ radical anion were resolved by Multivariate curve resolution (MCR) of TDRUV and TR^3 data sets. The RR spectra of $BP^{\bullet+}$ and $BP(T_1)$ correspond to nearly planar structures. The concentration decays fit a model of dispersed heterogeneous kinetics. At lower laser energy, $BP(T_1)$ was generated as major transient species. The energy transfer *via* T_1 occurs with rates not greater than $10^{-6}\,s^{-1}$. Photoionization is found to be the dominant phenomenon at higher pump laser energy. $BP^{\bullet+}$, Na_4^{3+} and $BP^{\bullet-}$ exhibit distinct decay behaviors with rates not lower than $10^{-3}\,s^{-1}$. In polar environment of $Na_{56}FAU$ supercage, the ejected electron is trapped as Na_4^{3+} cluster at low loading and as $BP^{\bullet-}$ at high loading. In the non-polar environment of FAU supercage, the ejected electron is captured by $BP(S_0)$ even at low loading. The effects of Si/Al ratio, extraframework cation and BP loading upon the energy and electron transfer rates were discussed according to BP photochemical behavior in solvents.

Keywords: Y zeolite; Biphenyl; Photolysis; Time resolved resonance Raman (TR^3) spectroscopy; Transient diffuse reflectance UV–vis absorption (TDRUV)

1. Introduction

Biphenyl (BP) and parent derivatives are produced in a variety of industrial and agrochemical processes. Efficient and low cost air cleaner systems have to be developed because the emissions in air represent a potential human health hazard particularly in work place atmosphere. Air purification is carried out by an adsorbent installed in a fluid flow system. The ultra stable Y-faujasite zeolite (USY) is a resistant inorganic adsorbent with well-known molecular sieves properties. So, this porous material can be used as efficient specific adsorbent for air cleaning systems. Hence, highly siliceous USY faujasitic zeolites are largely used in petroleum industry. The silica-rich Y zeolites abbreviated hereafter M_nFAU have the $M_n(AlO_2)_n(SiO_2)_{192-n}$ chemical composition per unit cell ($n = 0$–56) where M^+ is the counterbalancing cation. The M_nFAU porous structure consist of a 3D network of nearly spherical supercages of *ca.* 1.3 nm in diameter connected tetrahedrally through 0.74 nm windows. It was reported previously that biphenyl molecules are efficiently trapped from gas phase in dehydrated Y and USY zeolites [1]. The photolysis of loaded adsorbents of air cleaning apparatus is a promising way to decompose the occluded pollutants. There is evidence that the molecular sieves property of the zeolite is an important factor in photocatalysis efficiency, but the mechanism of zeolite participation in reactions remains incompletely elucidated [2]. The ever-increasing interest in photochemistry

* Corresponding author. Tel.: +33 3 20 43 69 62; fax: +33 3 20 43 67 55.
E-mail address: alain.moissette@univ-lille1.fr (A. Moissette).

1010-6030/$ – see front matter © 2007 Elsevier B.V. All rights reserved.
doi:10.1016/j.jphotochem.2007.09.018

of heterogeneous media has prompted many investigations of polyaromatics hydrocarbons (PAH), including BP adsorbed on inorganic surfaces including zeolites [3–10]. The zeolites are known to be very convenient hosts that are capable of modifying photochemical properties of guests from that exhibited in solutions [11–16].

Previous transient absorption studies have revealed several unique aspects of the photophysics and photochemistry of PAH occluded in zeolite networks, although controversial results have been obtained concerning particularly the fate of photoejected electron. Some years ago, transient diffuse reflectance laser photolytic studies of BP adsorbed using solvent in hydrated faujasitic $Na_{51}Y$ zeolite firmly established that biphotonic ionization generates $BP^{\bullet+}$ radical cation and that the ejected electron was captured by neutral BP to produce $BP^{\bullet-}$ radical anion at high loading [17]. Surprisingly, so far, no systematic kinetic study of BP photoproducts in dehydrated solvent-free silica-rich Y zeolites is available. Probably, the severe band overlaps make difficult the study of energy and electron transfer kinetics by transient absorption spectroscopy. Some opportunities to resolve this difficulty come from multivariate curve resolution (MCR) method. In addition, time resolved resonance Raman (TR^3) spectroscopy enables us to distinguish such molecular species from each other and to probe their structural changes along with time evolution [14,15].

The current investigation examines the energy and electron transfers induced by deep UV laser photolysis of biphenyl occluded within dehydrated silica-rich Y-faujasite (M_nFAU) zeolites and purely siliceous faujasites (FAU). The energy relaxation and charge recombination were explored using transient diffuse reflectance UV–vis absorption (TDRUV) and Time Resolved Resonance Raman (TR^3) in order to explore the 0.05–340 μs time range after flash excitation. The influences of aluminium content ($n = 0, 56$), charge-balancing cation ($M^+ = Na^+, K^+, Cs^+$), BP loading and laser pulse energy on the energy and electron transfer rates were investigated systematically. The MCR chemometric method was essential to resolve both the characteristic spectra and instantaneous molecular concentrations of transient species induced by laser pulses. The present work was initiated to gain a comprehensive understanding of the zeolite participation to the BP photochemical pathways generated by photolysis within polar M_nFAU and non-polar FAU microenvironments.

2. Experimental

2.1. Materials

The highly siliceous FAU or ultra stable USY or DAY zeolite $(SiO_2)_{192}$ (Si/Al = 100; micropore volume 0.29 cm^3/g) was kindly provided by Degussa. This dealuminated material is a Y-type zeolite having faujasite structure. The zeolite was prepared *via* a special $SiCl_4$ treatment that yields a Y zeolite in which almost all the Al atoms have been replaced by Si atoms. The properties of the Y framework have been fully retained, whereas medium size pores and defects are absent. Therefore, this type of zeolite exhibits enhanced temperature stability (>1000 K) and improved hydrophobic properties. The Na_{56}FAU ($Na_{56}Y$) zeolite $Na_{56}(SiO_2)_{136}(AlO_2)_{56}$ (Si/Al = 2.49; micropore volume 0.34 cm^3/g) was obtained from Union Carbide. $Na_4K_{52}(SiO_2)_{136}(AlO_2)_{56}$ and $Na_5Cs_{51}(SiO_2)_{136}(AlO_2)_{56}$ samples were obtained by cation exchange as reported previously [18]. Biphenyl ($C_{12}H_{10}$) was purchased from Merck-Schuchardt and was bisublimated. Pure and dry Ar and O_2 gas were used.

2.2. Sorption of biphenyl

Weighted amounts (∼1.4 g) of powdered hydrated zeolite $M_n(SiO_2)_{192-n}(AlO_2)_n$ (1–2 μm particle size) were introduced into an evacuable heatable silica cell. The sample was dried under vacuum (10^{-3} Pa) and heated stepwise to 773 K under air. O_2 was then admitted into the cell for 6 h at 773 K. The thermal treatment removed completely the water content and the organic impurities. Then, the sample was held under vacuum and cooled to room temperature under dry argon. Weighted amounts of bisublimated BP corresponding to 1–16 BP loading per unit cell were introduced into the cell under dry Ar and the powder mixture was shaken. After four weeks at 50 °C, the sample was held under vacuum for 3 h and then transferred under dry argon in a quartz glass Suprasil cuvette for diffuse reflectance UV–vis experiments or in cylindrical quartz tubes for TR^3 measurements.

2.3. Instrumentation

Elemental analyses (C, H, Al, Na, K, Cs) of the bare and loaded zeolites were obtained from the Service Central d'Analyse du Centre National de la Recherche Scientifique (Vernaison, France).

Ground state DRUV spectra were recorded at room temperature between 200 and 850 nm using a Cary 3 spectrometer equipped with integrating sphere. The corresponding bare zeolite was used as reference.

The experimental set-up of nanosecond diffuse reflectance laser photolysis, applicable to the detection of transient species (TDRUV) in optically inhomogeneous and light-scattering system was similar to that previously described [19]. It included an excimer laser as pump source (248 nm, 0.15–1.5 mJ, 20 ns, 0.3 Hz) and a pulsed xenon arc lamp as probe source allowing the analysis of an area of 1 cm^2. The decays at the different wavelengths were accumulated over ten laser pulses. The samples were shaken after every 10 laser shots to ensure a fresh sample surface was presented, although no colouring due to the formation of permanent photoproducts was evident. The TDRUV data were described by:

$$\text{Absorption } D(\lambda, t) = \frac{1 - R(\lambda, t)}{R_0(\lambda, t)} \quad (1)$$

where R and R_0 denote the intensities of the diffuse reflected light with and without excitation, respectively. In the case where the absorption of the transient D absorption is relatively low it has been shown that the concentration C of the transient will be directly proportional to D.

The nanosecond TR^3 set up has been detailed elsewhere [20,21]. It used excimer laser (Questek 2040) as pump excitation (248 nm, 1.5 mJ, 20 ns, 10 Hz), Nd:Yag + dye laser system (Quantel 581C, and TLD50) as probe pulse (370 nm, 1.5 mJ, 8 ns, 10 Hz), gated intensified diode array (20 ns gate) as detector, and home-built spectrometer. Both lasers are focused on an area of 1 mm^2. The spectral resolution and the analyzed field were about 8 and 1600 cm^{-1}, respectively, at 370 nm. The probe pulse was delayed with respect to the pump using home made generator. For measurements of solid samples a rotating cell was used and rejection of the elastic and inelastic diffused light was made by Notch filters.

2.4. Multivariate curve resolution

$\boldsymbol{D}(\lambda,t)$ represents the original data matrix with spectra in rows. Primarily, it is necessary to estimate the global rank of $\boldsymbol{D}(\lambda,t)$ to estimate the number of pure absorbing species (k) present in the whole data set (1) of the complex mixture. The $\boldsymbol{D}(\lambda,t)$ matrix is then decomposed into the following form:

$$\boldsymbol{D}(\lambda, t) = \boldsymbol{C}^k(t) \times \boldsymbol{S}_\lambda^{k\boldsymbol{T}} + \boldsymbol{E} \quad (2)$$

$\boldsymbol{C}^k(t)$ represents the 'spectral concentration' matrix. $\boldsymbol{S}_\lambda^{k\boldsymbol{T}}$ represents the transpose of $\boldsymbol{S}_\lambda^k$(spectral matrix) and $\boldsymbol{E}$ represents the residual error. SIMPLISMA approach was applied to resolve both the concentration matrix $\boldsymbol{C}^k(t)$ (k columns and t rows) and the spectral matrix $\boldsymbol{S}_\lambda^{k\boldsymbol{T}}$ of pure compounds (k rows and λ columns). $\boldsymbol{S}_\lambda^{k\boldsymbol{T}}$ and $\boldsymbol{C}^k(t)$ were calculated by standard matrix algebra according to the procedure detailed in the original publication without any prior information [22]. The difference between original and reconstructed data set lower than 5% relative root of sum of square differences (RRSSQ) provides a realistic picture of the components. The relative root of sum of square differences expresses the difference between the experimental data set $\boldsymbol{D}(\lambda,t)$ and the calculated data set $\boldsymbol{D}(\lambda,t)^{\mathrm{calc}}$. In a second step we used the multivariate curve resolution-alternating least squares (MCR-ALS) as a refined method. The optimization is carried out using $\boldsymbol{C}^k$ and $\boldsymbol{S}^{k\boldsymbol{T}}$ initial estimates obtained by SIMPLISMA approach. Convergence is achieved when the standard deviation σ of residuals with respect to experimental data are less than 3%. The relative molecular concentrations were estimated from the spectral concentration $\boldsymbol{C}^k(t)$ taking into account the molecular extinction coefficients of BP(T_1), $BP^{\bullet+}$ and $BP^{\bullet-}$ previously reported in solution [23–25].

2.5. Kinetic data processing

The simplest kinetic analysis of the $\boldsymbol{C}^k(t)$ decay have been tested in terms of mono, two or three exponentials. They do not reproduce accurately the decays. The concentration functions $\boldsymbol{C}^k(t)$ were accurately fitted using the Albery function. The Albery function takes into account the non-homogeneity of the material [26]. According to the model, the time-dependent absorption profile of a transient species can be represented by Eq. (3):

$$C(t) = \frac{\int_{-\infty}^{+\infty} \exp(-x^2)\ \exp(-\bar{k}t\ \exp(\gamma x))\,\mathrm{d}x}{\int_{-\infty}^{+\infty} \exp(-x^2)\,\mathrm{d}x} \quad (3)$$

where $\int_{-\infty}^{+\infty} \exp(-x^2)\,\mathrm{d}x = \sqrt{\pi}$.

If $\gamma = 0$ (no dispersion), the Eq. (3) is reduced to a first order kinetics: $C(t) = \exp(-\bar{k}\,t)$. $C(t)$ is the relative concentration, $\bar{k}$ is the average rate constant, and γ is the width of the distribution. Several attempts were made with other empirical or fractal approaches but they do not reproduce accurately the decays [27].

3. Results

3.1. Incorporation of BP in dehydrated silica-rich M_nFAU ($n = 0, 56$; $M = Na^+, K^+, Cs^+$)

Dehydrated M_nFAU with $M_n(AlO_2)_n(SiO_2)_{192-n}$ chemical formula per unit cell ($n = 0$, 56; $M = Na^+$, K^+, Cs^+) zeolites were loaded several months after mere mixing of dry zeolite powders with solid BP under inert atmosphere and without any solvent (see Section 2). The diffuse reflectance absorption spectra and off resonance Raman spectra were found to be in accurate agreement with complete incorporation as BP intact molecule in the void space of M_nFAU zeolites [1]. The BP sorption was successfully performed according to the following reaction:

$$m\mathrm{BP} + \mathrm{M}_n\mathrm{FAU} \rightarrow m\mathrm{BP@M}_n\mathrm{FAU} \quad (4)$$

$m = 1$, 2, 4, 8, 16 represents the BP loading per zeolite unit cell. The supercages are primary sites for occluded BP [1]. It was shown that there is no preferential BP sorption site in purely siliceous FAU supercages without any cations, whereas well-defined location sites are expected in $M_{56}FAU$ aluminated faujasite. In $M_{56}FAU$, BP lies in the super cavity in a twisted conformation with one phenyl group facially coordinated to the cations and the other phenyl group engaged in the 12-ring windows [1]. The formation of BP bimolecular aggregates within the same supercage is hindered by bulky M^+ cation [1] and occurs at relatively high loading. In contrast, in FAU zeolite without any cation, the aggregation occurs at low coverage. mBP@M_nFAU samples exhibit intense and broad UV absorption around 250 nm, these absorption bands are assigned to $S_3 \leftarrow S_0$ transition which are of the $\pi^* \leftarrow \pi$ type by comparison with previous results in solution [15]. However, the band shape and absorption coefficients were found to be slightly dependent on Si/Al, extraframework cation (M^+) and loading value (m) [1].

3.2. Transient diffuse reflectance UV–vis absorption

UV laser photolysis of mBP@M_nFAU samples was carried out within the contour of the $\pi^* \leftarrow \pi$ absorption using experimental setup detailed in the experimental section. The UV laser photolysis of bare M_nFAU did not lead to any TDRUV absorption with our experimental conditions. In contrast, significant TDRUV spectra were recorded in the 300–750 nm wavelength range when UV laser photolysis was carried out with mBP@M_nFAU samples. The $\boldsymbol{D}(\lambda,t)$ TDRUV spectra were

deduced through the $\boldsymbol{D}_\lambda(t)$ decays recorded at a wavelength value between 0.5 and 340 μs after the laser pulse. At short times, a very intense fluorescence is observed which prevents the recording below 0.5 μs.

3.2.1. *mBP@Na56FAU, effect of loading*

Many TDRUV spectra were recorded at different delay times after laser photolysis of 1 BP@Na_{56}FAU sample with different pulse energies (0.15, 0.8 and 1.5 mJ). Typical TDRUV spectra are exhibited in Fig. 1 where some absorption bands of $BP^{\bullet+}$ and $BP(T_1)$ mixtures were observed. It is clear also from examination of insert of Fig. 1 that a weak band about 490 nm is observed during 10 μs delay after the laser pulse. Calculated aliquots of water corresponding to 32 H_2O/UC loading were introduced in 1 BP@Na_{56}FAU sample to check the effect of residual water on BP photochemical behaviour. After an equilibrium period of several days, TDRUV spectra were recorded with identical experimental conditions. The resulting TDRUV spectra were found to be typical of $BP^{\bullet+}$ and $BP(T_1)$ species, however, the bands around 490 and 470 nm were not observed after addition of water. In contrast, supplementary broad band in the 750–800 nm region was observed. This finding is in accordance with the transient absorption spectra recorded after UV laser photolysis of BP incorporated using solvent in hydrated Na_{51}Y zeolite [17].

Typical TDRUV spectra recorded after the flash laser photolysis of the *m*BP@Na_{56}FAU samples with different loading values ($m = 4$, 8, 16) are exhibited in Fig. 2 where some absorption bands of $BP(T_1)$, $BP^{\bullet+}$, and $BP^{\bullet-}$ in mixtures can be discerned by comparison with transient spectra observed in solution.

The application of multivariate curve resolution (MCR) method data to the 3 $\boldsymbol{D}(\lambda,t)$ spectral sets (150 spectra) obtained with different pulse energy (0.15, 0.8, 1.5 mJ) during the photolysis of 1 BP@Na_{56}FAU sample resolved three independent spectra ($k = 3$) with residuals between experimental and calculated spectra less than 5% (Fig. 3a–c). The one band spectrum ($\lambda_{max} = 490$ nm) was assigned to Na_4^{3+} cluster (Fig. 3b) because of resemblance with transient spectrum recorded after high energy irradiation of dehydrated Y-faujasite [10]. The other resolved spectra (Fig. 3a and c) were successfully compared to UV–vis absorption spectra of $BP(T_1)$ and $BP^{\bullet+}$, transient species photogenerated by flash UV BP photolysis in solution [15,20,28]. The 360 nm band of spectrum in Fig. 3a was

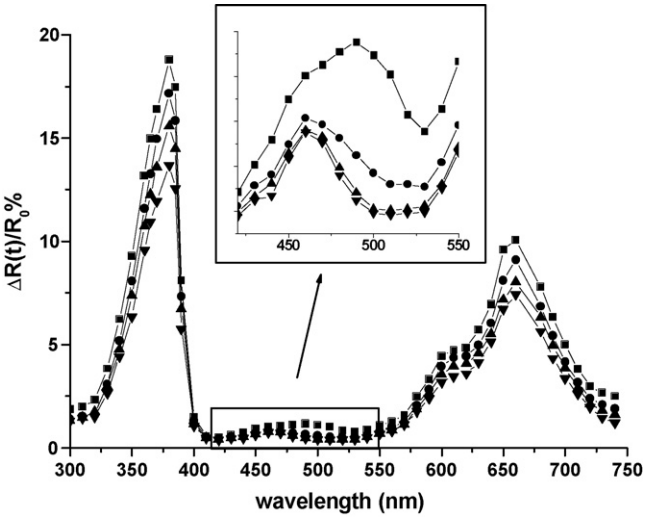

Fig. 1. TDRUV spectra recorded at different delays after pump excitation (248 nm, 20 ns, 1.5 mJ, 1 cm^2) of BP occluded in 1 BP@Na_{56}FAU: 1.5 (■), 10 (●), 30 (▲) and 90 μs (▼).

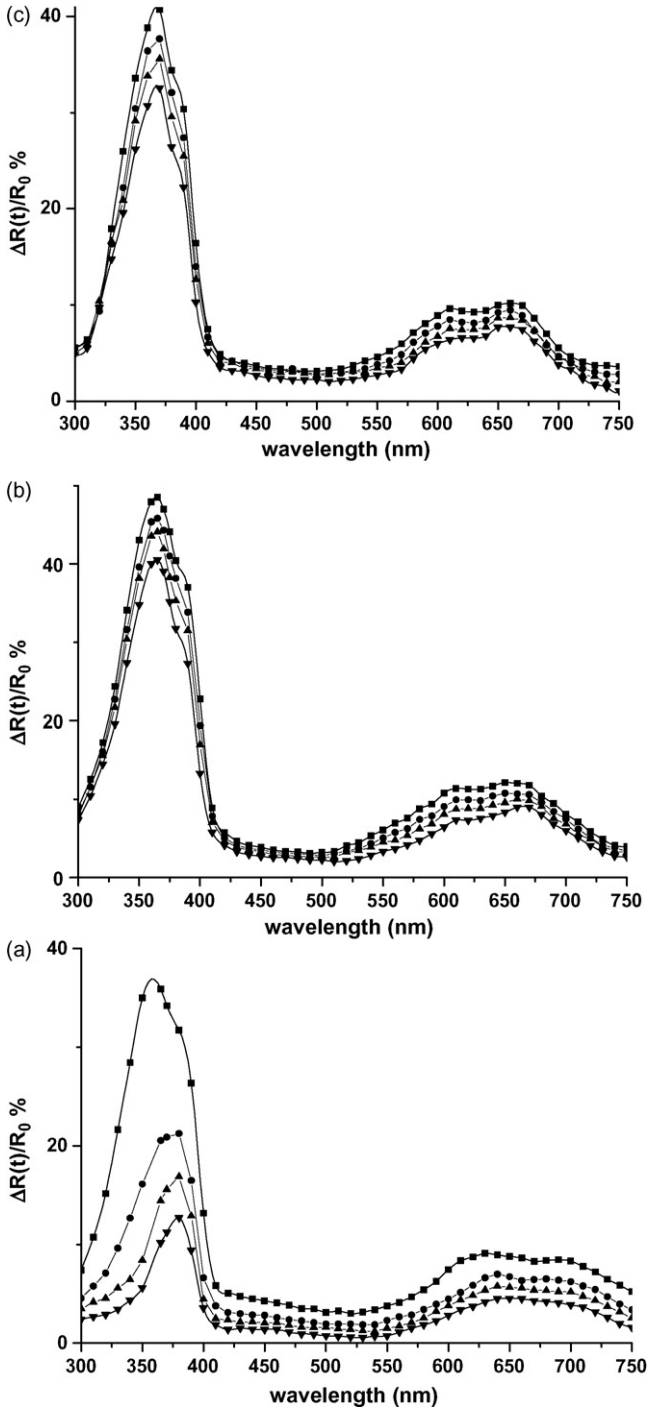

Fig. 2. TDRUV spectra recorded at different delays after pump excitation (248 nm, 20 ns, 1.5 mJ, 1 cm^2) of BP occluded in *m*BP@Na_{56}FAU: (a) $m = 4$; (b) $m = 8$; (c) $m = 16$ with 1.5 (■), 10 (●), 30 (▲) and 90 μs (▼).

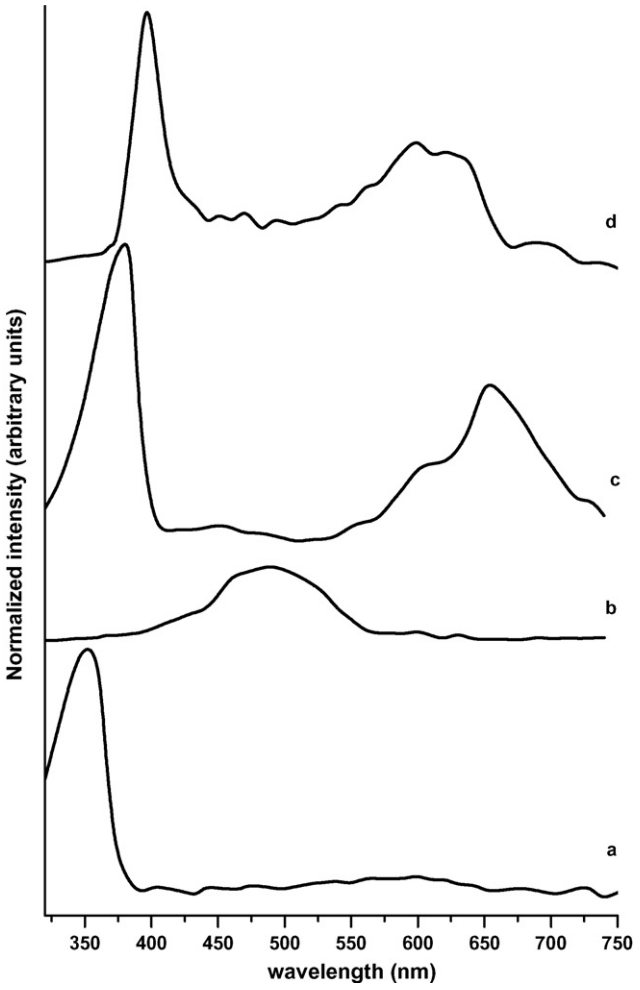

Fig. 3. UV–vis absorption spectra of transient species resolved by multivariate curve resolution (MCR) of transient diffuse reflectance UV (TDRUV) spectra recorded at different delays after pump excitation (248 nm, 20 ns, 0.2–1.5 mJ) of *m*BP@Na_{56}FAU: (a) BP(T_1), λ_{max} = 370 nm (35,000 M^{-1} cm^{-1}); (b) Na_4^{3+}; (c) $BP^{\bullet+}$ λ_{max} = 370 nm (12,000 M^{-1} cm^{-1}) and (d) $BP^{\bullet-}$ λ_{max} = 400 nm (10,000 M^{-1} cm^{-1}). Intensities are normalized by the MCR procedure. The molar extinction coefficients of transient species in zeolite are assumed to be analogous to those reported in solution.

assigned to $T_n \leftarrow T_1$ transition of BP(T_1), while the bands observed at 375 and 675 nm in spectrum of Fig. 3c were assigned to $^{*}BP^{\bullet+} \leftarrow BP^{\bullet+}$ transitions [14,15]. The careful comparison between $BP^{\bullet+}$ obtained in solution and in 1 BP@Na_{56}FAU reveals a supplementary band centred at 470 nm in the resolved $BP^{\bullet+}$ spectrum photogenerated in Na_{56}FAU. It should be noted that in the MCR procedure, only one species is resolved when the concentrations of two different species decrease or increase simultaneously. The weak band at 470 nm decreases concomitantly with the intense bands at 375 and 675 nm (Fig. 1), hence the weak band at 470 nm is resolved concomitantly with intense bands at 375 and 675 nm. This feature is not typical of $BP^{\bullet+}$ but typical of trapped electron in unknown site. The resolved spectrum shown in Fig. 3c is characteristic of $BP^{\bullet+}$@$Na_{56}FAU^{\bullet-}$ radical pair rather than isolated $BP^{\bullet+}$.

Three independent spectra were resolved by MCR of the 9 $\boldsymbol{D}(\lambda,t)$ spectral sets (500 spectra) recorded with m = 4, 8,16 and different pulse energy (0.15, 0.8, 1.5 mJ). The 3 spectra (k = 3) were straightforwardly attributed to BP(T_1), $BP^{\bullet+}$, and $BP^{\bullet-}$ (Fig. 3b–d). The third spectrum (Fig. 3d) contains two bands at 395 and 600 nm assigned to $^{*}BP^{\bullet-} \leftarrow BP^{\bullet-}$ transitions [14,29].

The MCR analysis of $\boldsymbol{D}(\lambda,t)$ spectra calculates also the relative spectral concentration $\boldsymbol{C}^k(t)$ of the absorbing transient species Na_4^{3+}, BP(T_1), $BP^{\bullet+}$, and $BP^{\bullet-}$ between 1 and 340 μs delay times despite severe spectral overlap. It should be noted that the extinction coefficients determined in solution $S_n \leftarrow S_0 \sim 18{,}000\ M^{-1}\ cm^{-1}$ at 260 nm, $T_n \leftarrow T_1 \sim 35{,}000\ M^{-1}\ cm^{-1}$ at 370 nm, $^{*}BP^{\bullet+} \leftarrow BP^{\bullet+} \sim 12{,}000\ M^{-1}\ cm^{-1}$ at 370 nm and $^{*}BP^{\bullet-} \leftarrow BP^{\bullet-} \sim 10{,}000\ M^{-1}\ cm^{-1}$ at 400 nm can provide a rough estimation of the relative $\boldsymbol{C}^k(t)$ molecular concentrations in the zeolites [23–25]. The Albery function provides an adequate description of the $\boldsymbol{C}^k(t)$ decays when nearly complete decays occur in the 0.5–340 μs range. Gaussian distribution kinetic model which was developed by Albery is based on a dispersion of first order rate constants $k = \bar{k}\exp(\gamma x)$, $\bar{k}$ is the average rate constant, and γ is the width of the distribution (see Section 2) [26]. The resulting $\bar{k}$ and γ values of all the successfully fitting procedures of the experimental decays are listed in Table 1 . The corresponding mean lifetimes are conventionally represented by $1/\bar{k}$. Nevertheless, when the lifetimes are less than 1 μs the $\bar{k}$ values are noted $>10^6\ s^{-1}$ in Table 1. In the same way, when the decays exceed largely 340 μs, the $\bar{k}$ values are noted $<10^3\ s^{-1}$.

The Fig. 4 is typical of BP(T_1), $BP^{\bullet+}$ and $BP^{\bullet-}$ concentration decays obtained with the 4 BP@Na_{56}FAU sample. The decays are successfully reproduced using the best γ and $\bar{k}$ fitting values listed in Table 1. The corresponding γ distribution coef-

Table 1
Average first-order rate constant $\bar{k}$ (s^{-1}) of the decays of the transient species generated by fast laser photolysis of biphenyl (BP) occluded in Y-faujasitic (*m*BP@M_nFAU, M = Na^+, K^+, Cs^+, n = 0, 56) zeolites

BP@unit cell	$\bar{k}$ BP(T_1) (s^{-1})	$\bar{k}$ $BP^{\bullet+}$ (s^{-1})	$\bar{k}$ Na_4^{3+} (s^{-1})	$\bar{k}$ $BP^{\bullet-}$ (s^{-1})
1 BP@Na_{56}FAU	$>10^6$	$\sim 3 \times 10^3$	3×10^5	
2 BP@Na_{56}FAU	$\sim 10^6$	7.5×10^4		
4 BP@Na_{56}FAU	6×10^5	2×10^5		4×10^5
8 BP@Na_{56}FAU	$\sim 10^5$	$<10^3$		$\sim 10^3$
16 BP@Na_{56}FAU	$\sim 10^4$	$<10^3$		$\sim 3 \times 10^3$
2 BP@K_{56}FAU	$\sim 10^6$	1×10^5		
2 BP@Cs_{56}FAU	5×10^5	5×10^4		
2 BP@FAU	$>10^6$	1×10^5		1×10^5

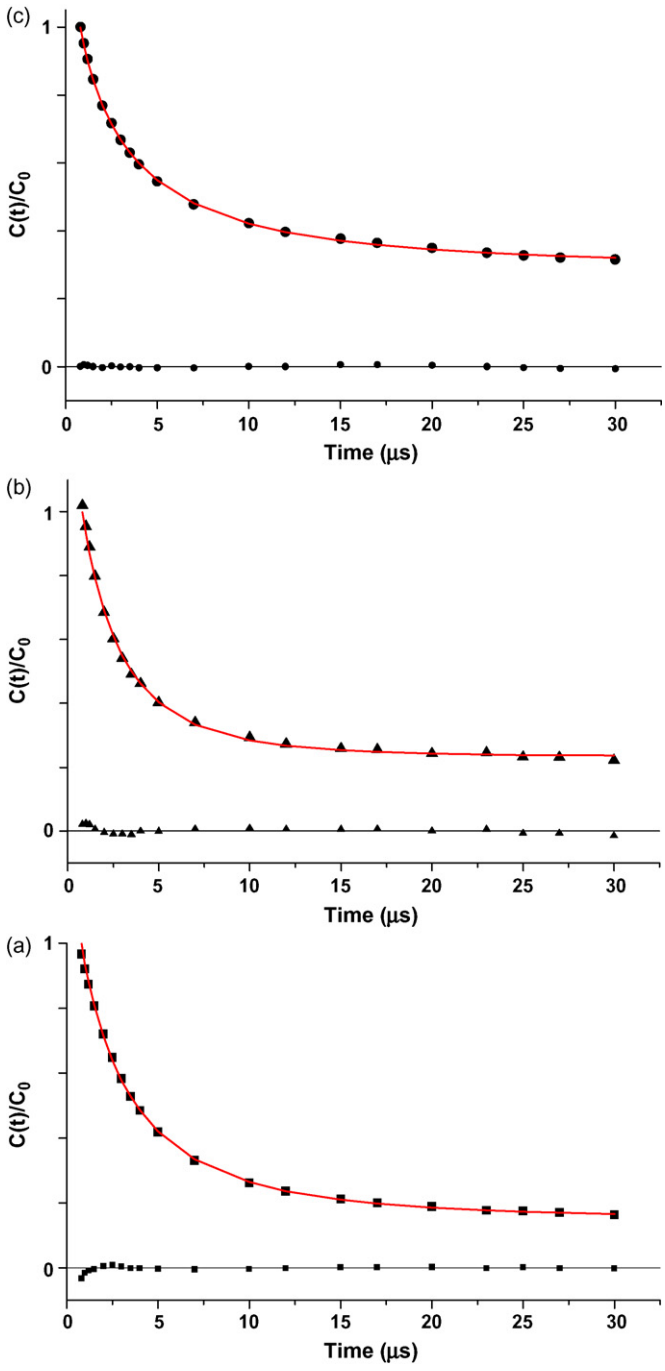

Fig. 4. Spectral concentration decay profiles of transient species generated by laser photolysis of 4 BP@Na_{56}FAU. Plots of residuals are indicated. (a) BP(T_1); (b) $BP^{\bullet+}$; (c) $BP^{\bullet}$; the relative $C(t)/C_0$ concentration values were extracted by MCR method from the experimental absorption decays. The solid lines represent the best calculated decays using the Albery function (see Section 2).

ficients were found to be between 1 and 5 and are in reasonable agreement with other heterogeneous photochemical reactions.

3.2.2. *mBP@M_{56}FAU (M = Na $^+$, K^+, Cs^+), effect of extraframework cation*

The TDRUV spectra recorded after laser photolysis of 2 BP@M_{56}FAU samples (M = Na^+, K^+, Cs^+) exhibit clearly the $BP^{\bullet+}$ spectral characteristics while supplementary bands of BP(T_1) were detected at shorter delay time (Fig. 5). No absorption was observed around 490 nm for M = K^+ and Cs^+.

The MCR processing of the $\boldsymbol{D}(\lambda,t)$ spectral set (150 spectra) recorded for 2 BP@Na_{56}FAU samples and with 0.15, 0.8 and 1.5 mJ laser pulse energy resolved three spectra straightforwardly attributed to Na_4^{3+}, BP(T_1) and $BP^{\bullet+}$ while MCR method extracts BP(T_1) and $BP^{\bullet+}$ spectra for M = K^+, Cs^+. The

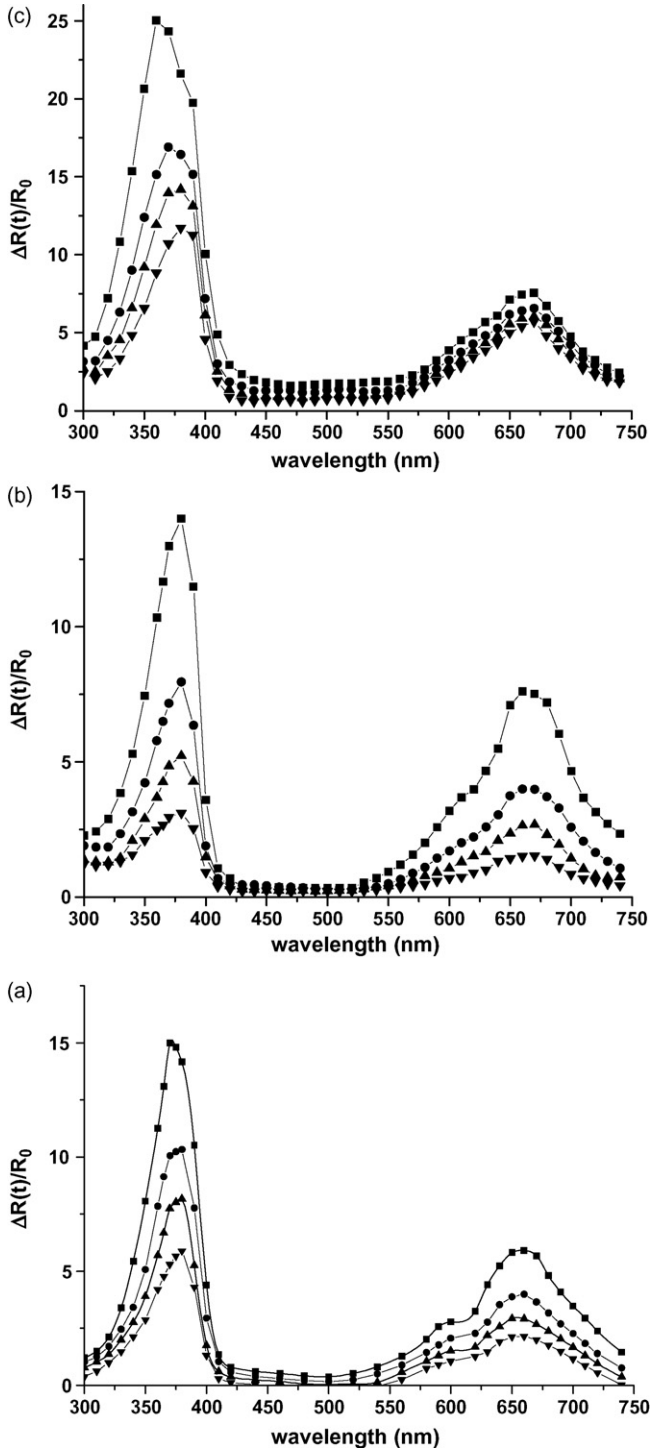

Fig. 5. TDRUV spectra recorded at different delays after pump excitation (248 nm, 20 ns, 1.5 mJ) of BP occluded in: (a) 2 BP@Na_{56}FAU; (b) 2 BP@K_{56}FAU; (c) 2 BP@Cs_{56}FAU: 1.5 (■), 5 (●), 10 (▲) and 30 μs(▼).

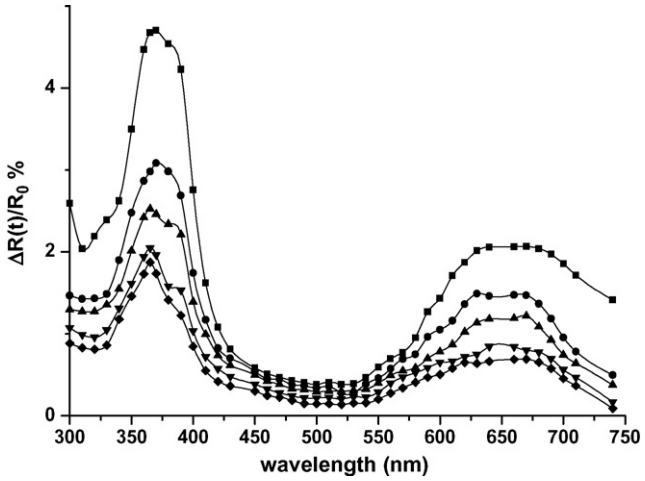

Fig. 6. TDRUV spectra recorded at different delays after pump excitation (248 nm, 20 ns, 1.5 mJ) of BP occluded in 2 BP@FAU: 1.5 (■), 5 (●), 10 (▲), 30 μs(▼) and (♦) 90 μs.

$BP^{\bullet+}$ decays are successfully reproduced using the best γ and $\bar{k}$ fitting values. The resulting $\bar{k}$ and γ values of all the successfully fitting procedures of the experimental decays are listed in Table 1.

3.2.3. *mBP@FAU, effect of Si/Al ratio and laser fluence*

The TDRUV spectra of *m*BP@FAU siliceous samples were recorded between 1 and 340 μs delay times. No absorption band was observed around 490 nm and no intense $BP(T_1)$ absorption was detected (Fig. 6) with delay time higher than 0.5 μs.

The data processing of the 6 $\boldsymbol{D}(\lambda,t)$ spectral sets (300 spectra) recorded with the *m*BP@FAU samples ($m = 1$, 2) and with 0.15, 0.8 and 1.5 mJ energy resolved only one spectrum ($k = 1$). The resolved spectrum does not correspond to any spectrum of known species listed in Fig. 3, but corresponds to $BP^{\bullet+}$–$BP^{\bullet-}$ mixtures as demonstrated by spectral decomposition. It should be noted that in the MCR procedure, only one species is resolved when the concentrations of two different species decrease or increase simultaneously. The $BP^{\bullet+}$ and $BP^{\bullet-}$ kinetic decays are identical and are treated as a $BP^{\bullet+}$–$BP^{\bullet-}$ ion pair recombination (Table 1).

The pump laser power dependence of the relative ratio $BP^{\bullet+}/BP(T_1)$ was examined at low BP loading in $Na_{56}FAU$ and with 1.5 μs delay time. The low BP loading in $Na_{56}FAU$ was chosen because laser pulse generates exclusively $BP^{\bullet+}$ and $BP(T_1)$. Except for high laser fluence for which saturation phenomena were observed, the $BP(T_1)$ concentration deduced from TDRUV measurements increases linearly with fluence whereas the $BP^{\bullet+}$ exhibits a concave curve as function of laser fluence. These behaviours are analogous to previously reported works [17,30] and suggest that $BP(T_1)$ is produced by monophotonic process and $BP^{\bullet+}$ is produced by biphotonic process.

3.3. *Time resolved resonance Raman (TR^3) scattering*

The above-described TDRUV results constitute a prerequisite for the TR^3 experiments. $BP(S_0)$ occluded in M_nFAU ($n = 0$, 56; $M = Na^+$, K^+, Cs^+) exhibit intense band absorption spectra around 250 nm. The UV absorption bands of $BP(T_1)$, $BP^{\bullet+}$ and $BP^{\bullet-}$ overlap in the same UV wavelength region, 360, 375 and 400 nm, respectively, whereas $BP^{\bullet+}$ and $BP^{\bullet-}$ exhibits overlapped visible absorption bands at 670 and 600 nm with weaker absorption coefficients (Fig. 3). The 248 nm pump wavelength was used to generate the transient species while the RR scattering of $BP(T_1)$, $BP^{\bullet+}$ and $BP^{\bullet-}$ was excited using the 370 nm probe wavelength (1.5 mJ, 8 ns). So far, attempts to record TR^3 probed at 625 nm failed [14]. The 370 nm probe wavelength excites also the off resonance Raman scattering of occluded $BP(S_0)$ in the ground state. Spectra acquired with only 370 nm probe pulses without any pump pulse showed exclusively the Raman features of occluded $BP(S_0)$. The spectra of $BP(S_0)$ occluded within M_nFAU ($n = 0$, 56; $M = Na^+$, K^+, Cs^+) zeolites spectra were found to be identical to that reported in a previous paper using NIR exciting line (1064 nm) [1]. For TR^3 experiments, pumping and probing beams were focused onto 1 mm^2 area of a rotating sample. Supplementary RR features were observed in TR^3 spectra recorded with both pump and probe beams for delay time from 50 ns to 100 μs. The TR^3 spectra were thus obtained by subtraction between these two spectra. It should be noted that the laser with 1.5 mW energy focused onto 1 mm^2 corresponds to higher energy density than used for transient absorption experiments (1 cm^2) and promotes the ionization.

3.3.1. *mBP@Na_{56}FAU, effect of loading*

TR^3 spectra (370 nm, 8 ns, 1.5 mJ) of transient species generated by laser photolysis (248 nm, 20 ns, 1.5 mJ) of *m*BP@Na_{56}FAU ($m = 2$, 4) samples were shown in Fig. 7. The RR band intensities of $BP(T_1)$ were observed to decrease with the pump probe delay times and with the pump energy. Two independent spectra were resolved from the 100 TR^3 spectra of the 2 spectral sets by MCR method with residuals between experimental and calculated TR^3 spectra less than 5%. The RR spectrum with bands at 1729, 1614, 1345, 1228, 1016, 991 and 735 cm^{-1} (Fig. 8b) was successfully assigned to $BP^{\bullet+}$ by comparison with TR^3 features of $BP^{\bullet+}$ (1725, 1615, 1342, 1224, 1018, 989 and 737) obtained in acetonitrile solution [15,20,28]. In the same way, the second set of bands (Fig. 8c) observed at 1575, 1479, 1370 and 967 cm^{-1} was assigned to $BP(T_1)$ and is in accurate agreement with TR^3 features (1570, 1476, 1366, 989) exhibited by $BP(T_1)$ photogenerated in cyclohexane solution [15]. No evidence of $BP^{\bullet-}$ radical anion was obtained [31]. It is probable that enhancement of the Raman scattering of $BP^{\bullet-}$ by resonance effect within the contour of the $BP^{\bullet-}$ absorption band (400 nm) is too weak to be detected using the 370 nm exciting line [15,32]. The striking analogies in frequency and in relative intensities of $BP(T_1)$ and $BP^{\bullet+}$ resonance Raman bands exhibited both in solution and in zeolite networks indicate no marked $BP(T_1)$ and $BP^{\bullet+}$ geometry change from solution to the zeolite porous space. As expected from previous theoretical calculations, $BP(T_1)$ exhibits planar quinone-like structure, $BP^{\bullet+}$ is found to be nearly planar with quinoidal structure and $BP^{\bullet-}$ is assumed to present also a planar structure [16,33]. The detailed assignment of the RR bands of $BP(T_1)$, $BP^{\bullet+}$ and $BP^{\bullet-}$ was achieved previously [34]. The $BP(T_1)$ temporal behavior was estimated at short delay time

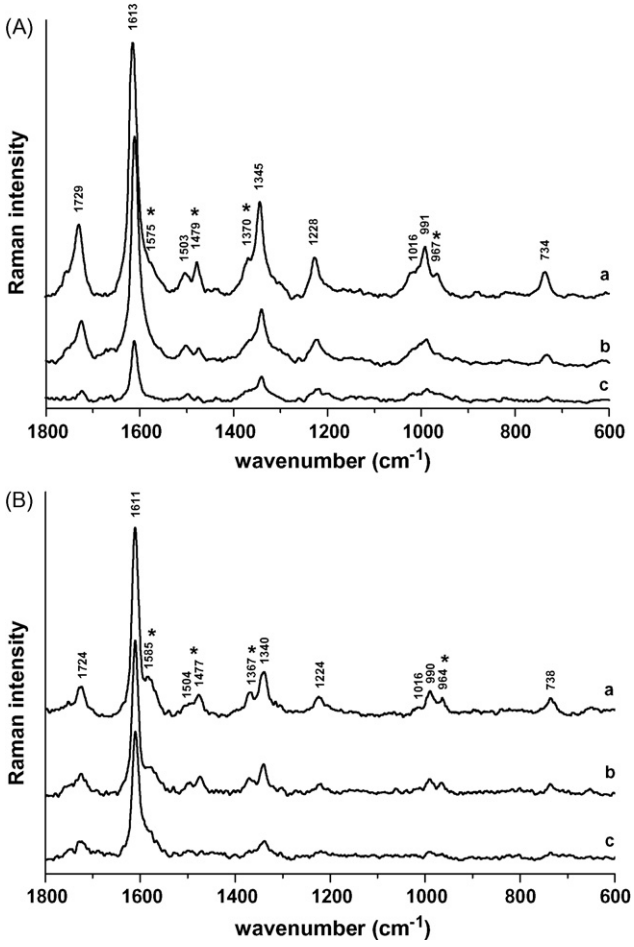

Fig. 7. TR^3 spectra (370 nm, 8 ns, 1.5 mJ) recorded at different time delays after pump excitation (248 nm, 20 ns, 1.5 mJ) of *m*BP@Na_{56}FAU: (A) $m = 2$; (a) 50 ns, (b) 1 μs and (c) 90 μs; (B) $m = 4$; (a) 50 ns, (b) 1 μs and (c) 90 μs. The unlabelled peaks correspond to $BP^{\bullet+}$; asterisks indicate the co-existing bands of $BP(T_1)$.

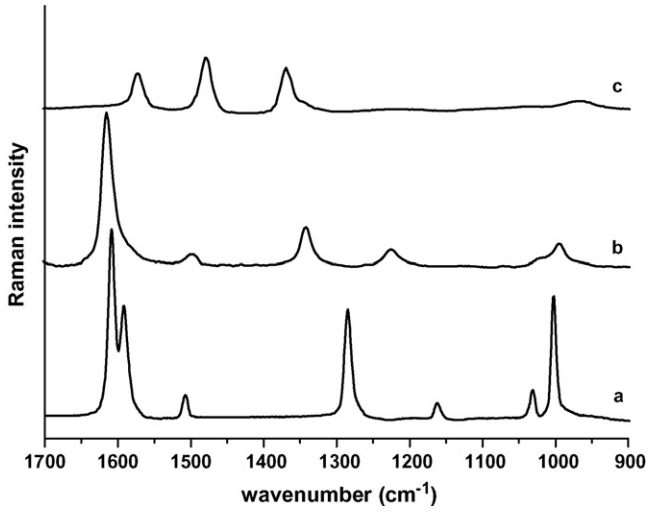

Fig. 8. Resonance Raman spectra of transient species resolved by multivariate curve resolution (MCR) of all transient time resolved resonance Raman (TR^3) spectra (370 nm, 8 ns, 1.5 mJ) recorded at different delays after pump excitation and different pump energy (248 nm, 20 ns, 0.2–1.5 mJ) of *m*BP@Na_{56}FAU: (a) $BP(S_0)$, (b) $BP^{\bullet+}$ and (c) $BP(T_1)$.

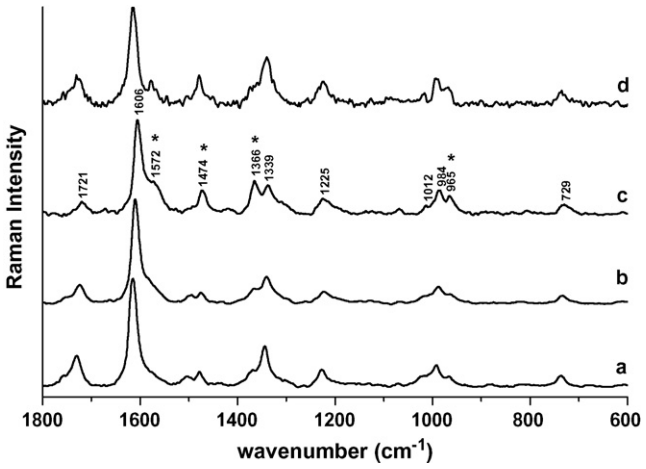

Fig. 9. Time resolved resonance Raman (TR^3) spectra (370 nm, 8 ns, 1.5 mJ) recorded at 50 ns time delay after pump excitation (248 nm, 20 ns, 1.5 mJ) of: (a) 2 BP@Na_{56}FAU; (b) 2 BP@K_{56}FAU; (c) 2 BP@Cs_{56}FAU; (d) 2 BP@FAU. The unlabelled peaks correspond to occluded $BP^{\bullet+}$; asterisks indicate the co-existing bands of occluded $BP(T_1)$.

(<1 μs) and the $BP^{\bullet+}$ rate constants were found to be analogous to that determined by transient absorption (Table 1).

3.3.2. *mBP@M_{56}FAU (M = Na^+, K^+, Cs^+), effect of extraframework cation*

The TR^3 spectra of 2 BP@M_{56}FAU samples (M = Na^+, K^+, Cs^+) exhibit mainly the $BP^{\bullet+}$ RR characteristics while supplementary $BP(T_1)$ weak bands were detected at shorter delay times (Fig. 9a–c). The rate constants extracted from the decays of the most prominent band (1606 cm^{-1}) of $BP^{\bullet+}$ were found to be in reasonable agreement with the values obtained by TDRUV absorption (Table 1). A qualitative estimation of the $BP(T_1)$ lifetime values comes from the intensities of shoulder at 1572 cm^{-1} of $BP(T_1)$. The $BP(T_1)$ decays in 2 BP@M_{56}FAU (M = Na^+, K^+, Cs^+) were found to increase as $Cs^+ < K^+ < Na^+$.

3.3.3. *mBP@FAU, effect of Si/Al ratio*

The TR^3 spectra of *m*BP@FAU samples ($m = 2$) exhibit mainly the $BP^{\bullet+}$ characteristics while supplementary $BP(T_1)$ weak bands were detected at short delay times (Fig. 9d) while no evidence of $BP^{\bullet-}$ was obtained with 370 nm probe wavelength. The rate constant extracted from the decay of the most prominent band (1606 cm^{-1}) of $BP^{\bullet+}$ was found to be in reasonable agreement with the value obtained by TDRUV absorption (Table 1) A qualitative estimation of the $BP(T_1)$ rate constant value comes from the intensities of shoulder at 1572 cm^{-1}.

4. Discussion

UV photolysis at lower laser fluence of occluded BP generates predominantly $BP(T_1)$ by a monophotonic process. In contrast, the photolysis at higher fluence promotes two-photon ionization. Therefore, T_1 population and ionization are two parallel photolytic processes which arise concurrently upon 248 nm excitation of $BP(S_0)$ occluded in silica-rich M_nFAU zeolites.

4.1. Energy transfer

As expected from photolysis studies in solution, population of the (BP)T_1 state occurs *via* rapid $S_1 \leftarrow S_3$ internal conversion, followed by $T_1 \leftarrow S_1$ intersystem crossing. Observation of BP(T_1)@M_nFAU, 50 ns after the $S_0 \rightarrow S_3$ excitation is consistent with short S_1 lifetime in the zeolite cavities (~16 ns in solution) and high $T_1 \leftarrow S_1$ quantum yield (0.8 in solution) [35] The structure of occluded BP(T_1) was found to be analogous to the quinone-like structure exhibited in solution with respect to the analogy of the RR spectra. BP(T_1) structure in zeolite cavities appears insensitive to the Si/Al ratio (n), the extraframework cation (M), and the loading value (m). In contrast, the entrapped BP(T_1) relaxation rate was found to depend on n, M and m. BP(T_1) exhibits significantly faster relaxation rate in mBP@M_nFAU than in solution. For example, BP(T_1) lifetime is markedly longer in solution, ~170 μs in cyclohexane and 40 μs in alcohols than in FAU, Na_{56}FAU, Na_{85}FAU and ZSM-5 zeolites (~1 μs) at low coverage [20,28]. The relaxation of triplet in the porous void space of zeolites can occur according to different channels. BP(T_1) decay takes into account BP(T_1) self-decay, quenching by ground state BP(S_0) and BP(T_1)–BP(T_1) annihilation [36,37]. It should be noted that BP(T_1)–BP(T_1) annihilation and quenching by ground state BP(S_0) depend on the BP mobility in the cavity network [12]. Reasonable correlations are observed between the BP(T_1) relaxation rates and BP(S_0) self-diffusivity coefficients in silica-rich M_nFAU [1]. In purely siliceous FAU, the statistic occupancy corresponds to 1 BP per 8 supercages at low loading ($m = 1$), but the mean-square displacements (MSD) during 1 μs corresponding to the mean BP(T_1) lifetime, were calculated to be ~25 nm^2 [1]. During this period, BP carries out large motions within FAU supercage and moves to many neighbour supercages, many possibilities of BP(T_1)–BP(T_1) annihilation and quenching by ground state BP(S_0) in neighbour cavities can occur. As reported previously, in Na_{56}FAU the BP motions were highly correlated to the motions of Na^+ cation through the Na^+ phenyl group interactions. At low coverage, with 1 BP per 8 supercages statistic occupancy, the MSD were calculated to be ~250 nm^2 during the BP(T_1) mean lifetime (~1 μs) [1]. Many possibilities of BP(T_1)–BP(T_1) annihilation and quenching by ground state BP(S_0) can occur during this period and explain the short BP(T_1) lifetime (~1 μs) in Na_{56}FAU at low loading. The different effects of charge-compensating cations on the efficiency of intersystem crossing and T_1 lifetime of PAH occluded in M_nFAU were demonstrated previously [9,38,39]. The weak increase of BP(T_1) lifetime (~2 μs) with bulky extraframework cation such as Cs^+ can be explained by the decrease of the BP diffusion coefficient. The weak MSD of BP (~10 nm^2 during 1 μs) in Cs_{56}FAU reduced the probabilities of BP(T_1)–BP(T_1) annihilation and quenching by ground state BP(S_0). In the same way, the increase of BP(T_1) lifetime in Na_{56}FAU as the BP loading increases can be related to the restriction of BP mobility at high loading rather than static occupancy. The accommodation of 2 BP per supercage hinders the BP diffusion at high loading and induces longer BP(T_1) lifetime [1]. For comparison, the BP(T_1) lifetime was reported to be markedly longer (~100 μs) at high BP loading ($m = 8$) in aluminium-rich Na_{85}FAU or X-faujasites [20].

4.2. Electron transfer

Excitation of BP occluded in silica-rich M_nFAU ($n = 0$, 56) at higher laser fluence results predominantly in the fast production of ionization products. According to TR[3] results, the $BP^{\bullet+}$ structure in zeolite cavities was found to be analogous to that exhibited in solution and appears insensitive to Si/Al ratio (n), extraframework cation (M), and loading value (m). The relaxation times of the photoinduced radicals ($BP^{\bullet+}$, Na_4^{3+} and $BP^{\bullet-}$) in the porous void space are in the 10–500 μs range. The relaxation processes in dehydrated solvent-free M_nFAU (Y)-faujasite imply electron transfers which were found to be different to that exhibited in solution. The $BP^{\bullet+}$, Na_4^{3+} and $BP^{\bullet-}$ relaxation rates depend on Si/Al ratio, extraframework cation (M) and BP loading. As originally shown by Thomas and co-workers, two-photon excitation of arenes included in dehydrated solvent-free NaY generates arene radical cations and Na_4^{3+} trapped electron ($M = Na^+$). This primary fast photoionization process was observed once again for BP occluded at low loading in strictly dehydrated Na_{56}FAU

$$BP@Na_{56}(AlO_2)_{56}(SiO_2)_{136} + 2h\nu \rightarrow BP^{\bullet+}@Na_{56}(AlO_2)_{56}(SiO_2)_{136} + \text{electron} \quad (5)$$

In purely siliceous FAU ($n = 0$) the photoejected electron is trapped by remaining BP(S_0) even at low loading

$$BP^{\bullet+}@(SiO_2)_{192} + \text{electron} + BP(S_0)@(SiO_2)_{192} \rightarrow BP^{\bullet+}BP^{\bullet-}@(SiO_2)_{192} \quad (6)$$

In Na_{56}FAU the ejected electron is trapped by Na^+ to form Na_4^{3+} clusters. The prolonged exposure of loaded zeolite to water was necessary to suppress the Na_4^{3+} clusters as reported for photoionization of biphenyl, pyrene and naphthalene occluded in hydrated Na_nFAU [17,40]. In anhydrous conditions the trapped electron migrates from Na_4^{3+} to another zeolite site according to

$$BP^{\bullet+}@Na_{56}{}^{\bullet-}(AlO_2)_{56}(SiO_2)_{136} \rightarrow BP^{\bullet+}@Na_{56}(AlO_2)_{56}(SiO_2)_{136}{}^{\bullet-} \quad (7)$$

The BP(S_0) ground state is restored in siliceous FAU through geminate recombination

$$BP^{\bullet+}BP^{\bullet-}@(SiO_2)_{192} \rightarrow 2BP@(SiO_2)_{192} \quad (8)$$

The $BP^{\bullet+}$ lifetime value (~10 μs) in hydrophobic FAU is markedly lower than that reported previously in non-polar beta zeolite for anthracene radical cation (~100 μs) [41].

In aluminated M_{56}FAU ($M = Na^+$, K^+, Cs^+) the charge recombination occurs as following

$$BP^{\bullet+}@M_{56}(AlO_2)_{56}(SiO_2)_{192-n}{}^{\bullet-} \rightarrow BP@M_{56}(AlO_2)_{56}(SiO_2)_{136} \quad (9)$$

The $BP^{\bullet+}$ lifetimes (~300 μs) are not found to be dramatically larger in the M_nFAU (0, 56; M = Na^+, K^+, Cs^+) faujasitic zeolites with large cavities than in solution (~70 μs in acetonitrile). In contrast, as demonstrated previously the medium pore (0.55 nm) aluminium-rich ZSM-5 zeolites hinder more efficiently the back electron transfer and stabilize $BP^{\bullet+}$ for more than 1 h at room temperature [42].

On increasing the BP loading in siliceous FAU the photolysis generates analogous phenomena as described in reactions (5), (6) and (8). In contrast, further increase in the BP loading to 4 BP per Na_{56}FAU unit cell generates concomitantly $BP^{\bullet+}$ and $BP^{\bullet-}$ under laser irradiation. The $BP^{\bullet-}$ radical anion is formed by intercepting photoejected electron before they are trapped in the framework zeolites. This explanation was previously used to interpret the laser photolysis of BP occluded in hydrated Na_{51}FAU and in dehydrated Na_{85}FAU [17,20]. It should be noted that the photoejected electron is efficiently trapped as $BP^{\bullet-}$ before any interception by Na^+ at more than 8 BP@Na_{85}FAU loading in X-faujasite.

$$BP^{\bullet+}@Na_{56}(AlO_2)_{56}(SiO_2)_{136} + \text{electron} + BP(S_0)@Na_{56}(AlO_2)_{56}(SiO_2)_{136} \rightarrow BP^{\bullet+}BP^{\bullet-}@Na_{56}(AlO_2)_{56}(SiO_2)_{136} \quad (10)$$

The $BP(S_0)$ ground state is restored in 8 $BP@Na_{56}(AlO_2)_{56}(SiO_2)_{136}$ through a reaction analogous to (8). The two ion radicals exhibit analogous but distinct decay behaviours from each other. It is probable that the recombination occurs *via* electron transfer process concerted with the electron donor ability of zeolites.

$$BP^{\bullet+}BP^{\bullet-}@Na_{56}(AlO_2)_{56}(SiO_2)_{136} \rightarrow 2BP(S_0)@Na_{56}(AlO_2)_{56}(SiO_2)_{136} \quad (11)$$

It was confirmed through the photoinduced electron transfer of BP in alcohols that $BP^{\bullet+}$ and solvated electron form by electron ejection from the S_1 state. The $BP^{\bullet-}$ anion forms as a result of the electron capture by $BP(S_0)$. Formation yields of the cation and anion radicals are determined by the solvent polarity and the electron mobility in the solvent, respectively [14]. The significant increasing of $BP^{\bullet+}$ and $BP^{\bullet-}$ lifetimes in Na_{56}FAU is explained by the low BP mobility at high loading [1].

5. Conclusions

The deep UV laser photolysis of biphenyl occluded in dehydrated silica-rich faujasitic Y (M_nFAU) and USY (FAU) zeolites generates biphenyl in the $BP(T_1)$ triplet state, $BP^{\bullet+}$ biphenyl radical cation, trapped electron, and $BP^{\bullet-}$ biphenyl radical anion.

The triplet state is generated mainly at low laser fluence. The molecular structure of $BP(T_1)$ is found to be planar as reported in solution. The relaxation times are found to be shorter in the Y and USY zeolites than in solution. It increases slightly in the 1–10 μs range as the loading increases, but remains shorter than in aluminium-rich X (M_{85}FAU) zeolites at high loading. The quenching occurs predominantly by the energy acceptor zeolite framework and is promoted by sorbate mobility in the cavity network. Photoionization to produce the planar $BP^{\bullet+}$ and photoejected electron is dominant at high pump laser fluence. In USY zeolite, the photoejected electron is trapped even at low loading as $BP^{\bullet-}$. In aluminated Y the electron trapping by $BP(S_0)$ is hindered by capture of ejected electron by the extraframework cation as Na_4^{3+} at coverage lower than 4 BP per Na_{56}FAU unit cell. The extraframework cation scavenger effect occurs at higher loading (8 BP/UC) in aluminium-rich X (Na_{85}FAU) zeolite with many cations. $BP^{\bullet+}$ and $BP^{\bullet-}$ exhibit distinct decay behaviors with rates lower than that reported in solution The significant increasing of $BP^{\bullet+}$ and $BP^{\bullet-}$ lifetimes in large cavity zeolites M_nFAU is explained by the low BP mobility at high loading. Nevertheless, the charge recombination of $BP^{\bullet+}$, Na_4^{3+}, $BP^{\bullet-}$ and trapped electron are not lower than 10^{-3} s^{-1} in large cavity faujasitic zeolites.

Acknowledgements

The Centre d'Etudes et de Recherches Lasers et Applications (CERLA) is supported by the Ministère chargé de la recherche, the région Nord/Pas de Calais, and the Fonds Européen de Développement Economique des Régions.

References

[1] I. Gener, G. Ginestet, G. Buntinx, C. Bremard, J. Phys. Chem. B. 104 (2000) 11656–11666.
[2] Y. Xu, C.H. Langford, J. Phys. Chem. B 101 (1997) 3115–3121.
[3] K.K. Iu, J.K. Thomas, J. Phys. Chem. 95 (1991) 506–509.
[4] K.K. Iu, X. Liu, J.K. Thomas, J. Photochem. Photobiol. A: Chem. 55 (1991) 377–386.
[5] F. Gessner, J.C. Scaiano, J. Photochem. Photobiol. A: Chem. 67 (1992) 91–100.
[6] J.K. Thomas, Chem. Rev. 93 (1993) 301–320.
[7] C. Brémard, G. Buntinx, V. De Waele, C. Didierjean, I. Gener, O. Poizat, J. Mol. Struct. 480–481 (1999) 69–81.
[8] H. Garcia, H.D. Roth, Chem. Rev. 102 (2002) 321–339.
[9] S.H. Hashimoto, J. Photochem. Photobiol. C: Photochem. Rev. 4 (2003) 19–49.
[10] J.K. Thomas, Chem. Rev. 105 (2005) 1683–1734.
[11] V. Ramamurthy, P. Lakshminarasimhan, C.P. Grey, L.J. Johnston, Chem. Commun. (1998) 2411–2424.
[12] J.C. Scaiano, H. Garcia, Acc. Chem. Res. 32 (1999) 783–793.
[13] V. Ramamurthy, J. Photochem. Photobiol. C: Chem. Rev. 1 (2000) 145–166.
[14] Y. Sasaki, H. Hamaguchi, J. Chem. Phys. 110 (1999) 9179–9185.
[15] G. Buntinx, O. Poizat, J. Phys. Chem. 91 (1989) 2153–2162.
[16] D. Pan, L.C.T. Shoute, D.L. Phillips, Chem. Phys. Lett. 316 (2000) 395–403.
[17] S. Hashimoto, T. Mutoh, H. Fukumara, H. Masuhara, J. Chem. Soc. Faraday Trans. 92 (1996) 3653–3660.
[18] C. Brémard, M. Le Maire, J. Phys. Chem. 97 (1993) 9695–9702.
[19] F. Wilkinson, C.J. Willsher, Appl. Spectrosc. 38 (1984) 897–901.
[20] I. Gener, G. Buntinx, A. Moissette, C. Bremard, J. Phys. Chem. B. 106 (2002) 10322–10329.
[21] G. Buntinx, G. Ginestet, I. Gener, G. Coustillier, C. Brémard, Laser Chem. 19 (1999) 325–327.
[22] W. Windig, B. Antalek, J.L. Lippert, Y. Batonneau, C. Brémard, Anal. Chem. 74 (2002) 1371–1379.
[23] D. Lavalette, C. Tetreau, Chem. Phys. Lett. 29 (1974) 204–209.
[24] O.M. Andreev, V.A. Smirnov, M.V. Alfimov, J. Photochem. 7 (1977) 149–156.
[25] C. Takahashi, S. Maeda, Chem. Phys. Lett. 24 (1974) 584–588.

[26] W.J. Albery, P.N. Bartlett, C.P. Wilde, J.R. Darwent, J. Am. Chem. Soc. 107 (1985) 1854–1858.
[27] P.P. Levin, L.F. Vieira Ferreira, S.M.B. Costa, Langmuir 9 (1993) 1001–1008.
[28] I. Gener, G. Buntinx, C. Brémard, Angew. Chem. Int. Ed. 38 (1999) 1819–1822.
[29] T. Shida, Electronic Absorption Spectra of Radical Ions, Elsevier, Amsterdam, 1988.
[30] F. Wilkinson, D.W. Worrall, S.L. Williams, J. Phys. Chem. 99 (1995) 6689–6696.
[31] V. Aleksandrov, Y.S. Bobovich, Y.G. Maslov, A.N. Sidorov, Opt. Spectrosc. 38 (1975) 685–688.
[32] C. Kato, H. Hamaguchi, M. Tasumi, Chem. Phys. Lett. 120 (1985) 183–187.
[33] S.Y. Lee, Bull. Korean Chem. Soc. 19 (1998) 93–98.
[34] C. Lapouge, G. Buntinx, O. Poizat, J. Mol. Struct. 651–653 (2003) 747–757.
[35] I.S. Berlman, J. Phys. Chem. 74 (1970) 3085–3093.
[36] J. Saltiel, G.R. Marchand, W.K. Smothers, S.A. Stout, J.L. Charlton, J. Am. Chem. Soc. 103 (1981) 7159–7164.
[37] M.J. Kremer, K.A. Connery, M.M. DiPippo, J. Feng, J.E. Chateauneuf, J.F. Brennecke, J. Phys. Chem. A 103 (1999) 6591–6598.
[38] V. Ramamurthy, J.V. Casper, D.F. Eaton, E.W. Kuo, D.R. Corbin, J. Am. Chem. Soc. 114 (1992) 3882–3892.
[39] F.L. Cozens, H. Garcia, J.C. Scaiano, J. Am. Chem. Soc. 115 (1993) 11134–11140.
[40] M. Alvaro, A. Corma, B. Ferrer, H. Garcia, E. Palomares, PCCP 6 (2004) 1345–1349.
[41] E.H. Ellison, J. Phys. Chem. B 109 (2005) 20424–20432.
[42] I. Gener, A. Moissette, C. Brémard, Phys. Chem. Chem. Phys. 6 (2004) 3732–3738.